Nominal *vs* Local Shot-Peening Effects on Fatigue Lifetime in Ti-6Al-2Sn-4Zr-6Mo at Elevated Temperature

S.K. JHA, R. JOHN, and J.M. LARSEN

A study is presented of elevated temperature (260 °C) fatigue lifetime variability in the shot-peened condition of the $\alpha + \beta$ titanium alloy, Ti-6Al-2Sn-4Zr-6Mo. It is shown that failures separate into two distributions: (1) governed by the nominal residual stress (RS) profile, promoting subsurface crack initiation and longer lifetimes; and (2) life-limiting behavior that is controlled by localized material-shot-peening interaction. In the residual-stress-free condition, failures occurred predominantly by surface crack initiation at the microstructural scale, on the order of 10 μm, by crystallographic facet formation in one or a few α particles or colonies. This mechanism was mitigated under the nominal shot-peening (SP) RS profile, producing failures initiating from the subsurface region by crystallographic faceting spread over a significantly larger area (equivalent diameter of about 100 to 200 μm) than in the absence of RS. Although the microstructure-scale surface-crack initiation was suppressed, the life-limiting failures under SP continued to occur by surface initiation, but through an apparently larger crack initiation size by formation of a flat, noncrystallographic fracture area (equivalent diameter of about 60 to 200 μm) at the crack origin.

DOI: 10.1007/s11661-009-9931-0

I. INTRODUCTION

COMPRESSIVE-RESIDUAL-STRESS-PRODUCING treatments, including shot peening (SP), have been shown to enhance the resistance of a surface to fatigue crack initiation and propagation.[1–5] Often, the benefit to lifetime is measured in terms of the mean-fatigue behavior, which exhibits significant improvement upon SP due to, depending on the loading conditions, a shift in the failure initiation from the surface to the subsurface regions[6–8] or delayed crack initiation or retardation of crack growth from the surface.[9 12] The driving force for crack initiation is thought to be reduced due to the uniform distribution of immobile dislocations in the peened surface layer, which restricts the motion of dislocations and the development of intense slip bands during fatigue loading.[13,14] Along similar lines, others have attributed the delay in crack initiation to a decreased level of plastic strain accumulation in the work-hardened surface material.[4,14] The retardation of crack propagation or crack arrest is related to the significant reduction in the effective stress intensity factor range under the compressive residual stress (RS) profile[9,10,15,16] as well as the decreased crack-tip plasticity due to work hardening.[17]

It is also well documented that the degree of influence on the lifetime is strongly dependent on the stress level and temperature regime,[7,8,11,18,19] as well as the stress gradient.[9] In particular, the subject of RS relaxation has been given widespread attention[7,9,20–22] in this regard. At cyclic stress levels above the material yield strength, under the global-yield condition, or at high temperatures, the benefit of SP could decrease due to relaxation of the RS profile.[7,14,23,24] At lower stress levels, *i.e.*, the long-lifetime regime, the SP effect may be reduced if failure would have predominantly occurred by subsurface crack initiation in an otherwise RS-free condition[18] and due to the dominant contribution of crack initiation to the total lifetime.[4] The latter is typically a more influential factor in notch fatigue[2,25] than smooth fatigue. The SP-induced surface roughness, which has also been given important consideration in several studies,[7,8,26] can have a competing influence on the beneficial effects of the compressive stress and the cold work level, especially under thermal-mechanical conditions where the RS profile may significantly relax.

It is clear that the response of an SP-induced (or any other treatment) RS profile to the variables encountered in service and the resulting effect on lifetime must be understood in order to accurately incorporate it in life prediction. Several lifing approaches incorporating these mechanisms have been proposed,[4,9,10,15] where the fatigue lifetime behavior with respect to the global RS and cold work levels has been studied. In addition, another pervasive consideration in life prediction is the role of surface treatment in the lifetime distribution, in addition to the mean-lifetime effects. However, this aspect has not been sufficiently addressed in past SP studies. In the RS-free condition, for instance, it has been demonstrated that the average microstructure, or the distribution about the mean characteristics, is not an

S.K. JHA, Research Scientist, is with Universal Technology Corporation, Dayton, OH 45432. Contact e-mail: sushant.jha@wpafb.af.mil R. JOHN, Principal Materials Research Engineer, and J.M. LARSEN, Senior Scientist, are with the United States Air Force Research Laboratory, AFRL/RXLMN, Materials and Manufacturing Directorate, Wright-Patterson Air Force Base, OH 45433.
Manuscript submitted September 15, 2008.
Article published online August 25, 2009

Report Documentation Page

Form Approved
OMB No. 0704-0188

1. REPORT DATE	2. REPORT TYPE	3. DATES COVERED
NOV 2009		**00-00-2009 to 00-00-2009**

4. TITLE AND SUBTITLE	5a. CONTRACT NUMBER
Nominal VB Local Shot-Peening Effects on Fatigue Lifetime in Ti-6AI-2Sn-4Zr-6Mo at Elevated Temperature	5b. GRANT NUMBER
	5c. PROGRAM ELEMENT NUMBER
6. AUTHOR(S)	5d. PROJECT NUMBER
	5e. TASK NUMBER
	5f. WORK UNIT NUMBER
7. PERFORMING ORGANIZATION NAME(S) AND ADDRESS(ES) **Air Force Research Laboratory,AFRL/RXLMN,Materials and Manufacturing Directorate,Wright Patterson AFB,OH,45433**	8. PERFORMING ORGANIZATION REPORT NUMBER
9. SPONSORING/MONITORING AGENCY NAME(S) AND ADDRESS(ES)	10. SPONSOR/MONITOR'S ACRONYM(S)
	11. SPONSOR/MONITOR'S REPORT NUMBER(S)

12. DISTRIBUTION/AVAILABILITY STATEMENT
Approved for public release; distribution unlimited

13. SUPPLEMENTARY NOTES

14. ABSTRACT

15. SUBJECT TERMS

16. SECURITY CLASSIFICATION OF:			17. LIMITATION OF ABSTRACT	18. NUMBER OF PAGES	19a. NAME OF RESPONSIBLE PERSON
a. REPORT	b. ABSTRACT	c. THIS PAGE			
unclassified	**unclassified**	**unclassified**	**Same as Report (SAR)**	**10**	

accurate predictor of the lifetime variability.[27,28] In particular, the lower tail of lifetime has been shown to be often controlled by an extreme microstructural configuration or arrangement, which otherwise has a small probability of occurrence and may not be accounted for in conventional statistical characterization of microstructure.[29] In aerospace applications, many parts are surface treated to impart surface RSs, and it is important to determine if in that condition the life-limiting behavior can be accurately extrapolated from the nominal fatigue behavior deduced from the characterization of the RS profile.

In light of the preceding discussion, the objective of this article is to analyze the distribution in lifetime under a relevant SP condition at a given stress level and temperature in the turbine engine alloy Ti-6Al-2Sn-4Zr-6Mo (Ti-6-2-4-6). The experimental conditions were chosen to target a regime where failure is invariably caused by surface crack initiation in the absence of surface treatment, and also to avoid a regime where the RS may significantly relax. It is shown that lifetime variability separates into two behaviors: one driven by the nominal RS level and the other a life-limiting behavior controlled by the local, material-SP interaction effects. This nominal *vs* life-limiting approach to measuring the benefit of a surface treatment can be of key significance in accurately incorporating the RS in probabilistic life prediction.

II. MATERIAL AND EXPERIMENTAL PROCEDURE

A. *Material*

The material in this study was the $\alpha + \beta$ titanium alloy, Ti-6-2-4-6, in the duplex microstructural condition. Two variants of the microstructure, which differed moderately in terms of optical characterization, were considered. These were designated as microstructures A and B and are presented in Figures 1(a) and (b), respectively. As shown, microstructure B had a higher volume fraction of equiaxed primary-α particles, about 33 pct. Microstructure A had approximately 19 pct volume fraction of primary α. Microstructure B displayed a relatively smaller aspect ratio of secondary lath-α. These microstructures also varied in terms of their crystallographic texture, as reported elsewhere.[27] Besides these characteristics, both microstructures consisted of microtextured regions[31] in that regions of similarly oriented α phase were present. The microtexturing was further found to be related to the underlying β grains. Preliminary study indicated that the two microstructures differed in terms of the size of microtextured regions, which in microstructure A was on the order of 0.5 to 1 mm but existed on a smaller size scale in microstructure B.

The tensile behavior at 260 °C of the two microstructures was nominally similar, as depicted by Figure 2. The 0.2 pct yield strengths were about 850 and 825 MPa, and the ultimate tensile strengths were about 1040 and 1012 MPa, respectively, for microstructures A and B (Figure 2).

B. *Experimental Procedure*

The fatigue specimens were electrodischarge machined with the length aligned in the circumferential orientation from forgings of the two microstructures. The final machining was done by low stress grinding (LSG). The round-bar geometry with the gage diameter of about 4 mm and the gage length of about 12.5 mm was employed. In order to produce a residual-stress–free surface, the specimens were electropolished to remove about 50-μm layer from the surface. For the samples used in the RS study, SP was performed on the LSG surface.

The fatigue experiments were conducted in an automated servohydraulic test system. Axial, load-controlled

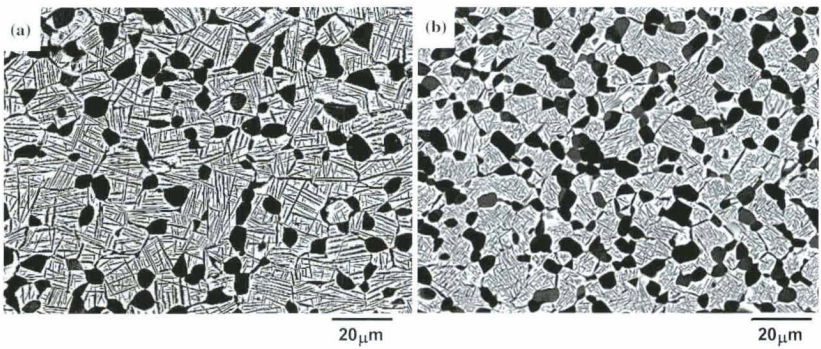

Fig. 1 –Microstructures of the Ti-6-2-4-6 alloy considered in the study. (*a*) Microstructure A consisting of equiaxed primary-α (~19 pct volume fraction) and high aspect ratio lath-α/transformed-β colonies. (*b*) Microstructure B consisting of a relatively higher volume fraction (~33 pct) of primary-α and a smaller aspect ratio of lath-α.

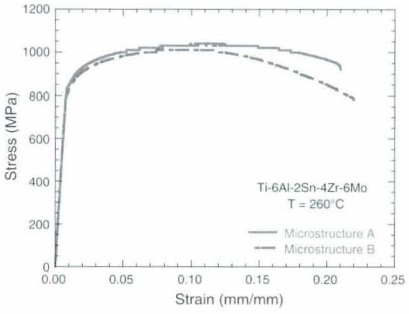

Fig. 2 Tensile behavior of Ti-6-2-4-6 microstructures at 260 °C.

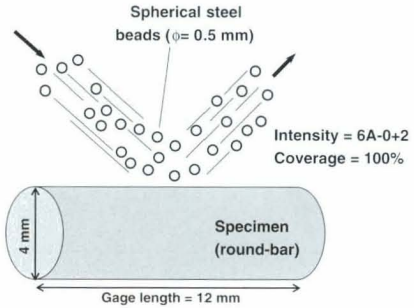

Fig. 3—Schematic of the peening configuration in the present study. The relative dimensions of shots and specimen are drawn to scale.

fatigue at a frequency of 20 Hz and stress ratio (R) of 0.05 was employed. A constant amplitude sine-wave profile was applied with the maximum stress of 860 MPa. The test temperature was 260 °C and the atmosphere was lab air.

Elevated temperature experiments were accomplished in two types of test configurations: (1) a resistance heating furnace, using a button-head type gripping assembly, and (2) a four-zone quartz-lamp heating system with collet grips. In (1), two thermocouples were welded at the gage ends of the specimen for temperature control. In (2), four loop thermocouples were mounted along the gage length, which independently controlled the temperature in each zone. Additionally, two thermocouples were welded in the upper and lower shoulder regions of the specimen, which were maintained at the test temperature with the help of resistance coils. The quartz-lamp system was employed in all experiments involving SP. The heating rate and the soaking time at temperature before commencing a test were kept constant across all tests to minimize any variation in the thermal relaxation of RS between specimens prior to cycling.

The microstructural characterization was done in a field-emission scanning electron microscope (SEM) in the backscattered electron mode. The same SEMs were also used in the fracture surface analysis. The crack initiation area was determined from the convergence of the radial crack-growth marks. The crack initiation area was outlined and measured using the ImagePro image analysis program (MediaCybernetics, Bethesda, MD). The spatial angles of crack initiation facets were measured by quantitative tilt fractography with the aid of the MeX image analysis program. This required the input of stereo-image pairs (at 0 and 6 deg tilts) of the crack initiation region at a fixed working distance, which were acquired in the SEM.

III. SURFACE TREATMENT, RS, AND RELAXATION

The SP produces the compressive RS by plastically deforming the surface layer, which is accomplished by impacting the work piece with a hard medium (or shots).[1] The SP process variables need to be closely controlled to obtain the targeted RS profile, as well as a uniform surface condition. The peening configuration in the present study is schematically illustrated in Figure 3, where the relative dimensions of the specimen and the shots have been drawn to scale. For the purpose of this study, typical SP parameters applicable to titanium surfaces were invoked. In this case, spherical steel beads of 0.5-mm diameter were used as the impacting medium. The peening intensity was 6A-0 + 2A (Almen A scale per the ASME specification), and the coverage was 100 pct. Each sample was subjected to an inspection by a fluorescent tracer coating method to ensure that the coverage was complete. The peening was done on the previously LSG surface, which ensured uniformity of surface between specimens prior to peening. In order to minimize any process variability, specimens from the two microstructures were randomized and peened in a single batch.

The baseline RS profile produced by the SP treatment, measured in an untested sample, is presented in Figure 4. The RS levels were measured by the X-ray diffraction technique[32] *via* destructive layer removal. The figure depicts that a compressive RS of about 860 MPa was produced at the surface, with the maximum compressive stress reaching about 1000 MPa just below the surface (~20 μm). The depth of the compressive layer was about 160 μm. It is well known that the RS field relaxes upon fatigue or with exposure to elevated temperature.[7,12,20–22] The relative contributions of the two primary components of the relaxation process, mechanical and thermal, are strongly dependent on the initial RS profile, the temperature, and the applied stress level.[7,21,22] In general, the mechanical relaxation is attributed to stress redistribution over the specimen cross section due to cyclic softening of the material.[22] The thermal relaxation of RS has been related to the healing of crystalline defects, which are produced during SP by thermally activated processes.[15,21] A detailed discussion of these relaxation effects in Ti-6-2-4-6 is the subject of another article.[24]

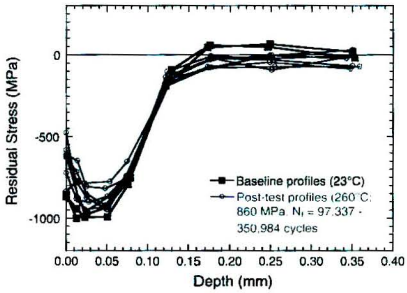

Fig. 4—Baseline and relaxed (postcompletion of test) RS profile in Ti-6-2-4-6.

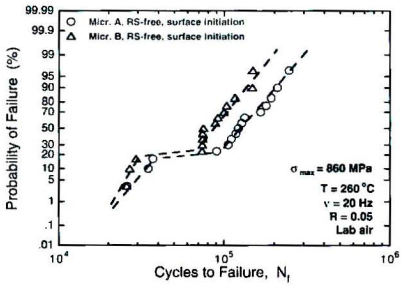

Fig. 5—Fatigue variability behavior in Ti-6-2-4-6 in the RS-free condition at 260 °C.

where a systematic study of the influence of thermal exposure (up to 100 hours) *vs* fatigue loading as a function of temperature is provided. Here, the relaxed RS profile was measured upon completion of a fatigue test (presumably containing contributions from both factors), and this is shown in Figure 4.[24] The measurements were made in the gage section of samples with failure lifetime in the range of 97,337 to 350,984 cycles. The relaxed profiles shown in the figure represent the measurements from seven samples (six of microstructure A and one of microstructure B). A moderate degree of relaxation, especially in the near surface regions, is clearly evident here (Figure 4), although there was a considerable degree of variability between profiles. The figure also clearly demonstrates that the stress level and temperature were suitable to retain a significant amount of compressive stress in the sample, about 79 to 95 pct of the subsurface maximum RS in the baseline profile.

IV. RESULTS AND DISCUSSION

A. *Fatigue Variability Behavior in the RS-Free Condition*

The fatigue variability behavior of microstructures A and B at 260 °C in the RS-free (*i.e.*, electropolished) condition is presented in Figure 5. A more detailed discussion in terms of the effect of microstructure and temperature on the lifetime variability has been provided in Reference 27. In the figure, the experimental points have been plotted on the cumulative distribution function scale using the lognormal model. In both microstructures, a steplike behavior of data, as illustrated by the dashed lines, was observed. In Ti-6-2-4-6, this has been attributed to a superposition of the crack-growth-controlled (life-limiting) mechanism with the crack-initiation-dominated (mean) behavior.[27] The effect of microstructural and extrinsic variables on the lifetime variability can then be modeled in terms of the distinct influence of these on the crack initiation and growth regimes, affecting the degree of separation between the two superimposing behaviors, as shown in References 27 through 29.

Figure 5 also points to the very similar lower tail of the lifetime distribution (the observed minimum lifetimes being 25,851 *vs* 25,744 cycles in microstructures A and B, respectively) in the two microstructures, which can be attributed to their very similar small and long crack growth behavior.[27] At the same time, the longer mean lifetime (about 125,945 *vs* 83,206 cycles, respectively), as well as the increased lifetime variability in microstructure A, was suggested to arise from a separation between the crack-initiation-controlled responses of the two,[27,29] due to a much greater sensitivity of the crack initiation regime to even a moderate degree of microstructural modification. Besides microstructure, the effect of stress level and temperature on lifetime variability can also be understood in terms of different rates of influence of these variables on the crack-growth- and crack-initiation-controlled responses,[27,30] therefore producing their separation or convergence.

B. *Failure Mechanism in the RS-Free Case*

In terms of the crack-initiation mechanism, in the RS-free condition (*i.e.*, electropolished surface) failures occurred exclusively by surface initiation, as indicated in Figure 5. By surface initiation, it is implied that the crack initiating microstructural feature either intersected the surface or was within one primary-α diameter (about 4 μm) from the surface. A typical crack origin in the RS-free case in microstructure B is shown in Figure 6. Quantitative details on the crack initiation features, in terms of their size and angle with respect to the loading axis, are provided in Section IV–C. As shown in Figure 6(a), crack initiation could characteristically be traced to facet formation in an equiaxed primary-α (α_p) particle on the size scale of approximately 10 μm. In some cases, two or three adjacent α_p or colony facets represented the surface crack initiation site. Measurements of the facet angle with respect to the loading axis revealed that the facet planes were oriented for shear or slip deformation. This is also evident in the tilted

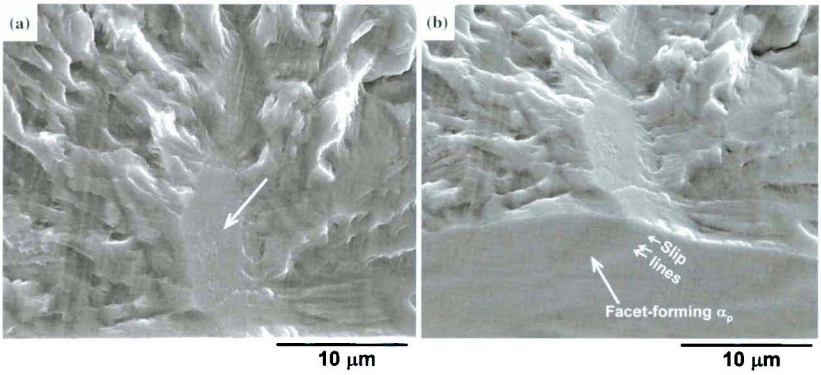

Fig. 6—Crack initiation characteristics in the RS-free condition at 260 °C in microstructure B. Crack initiation facet shown at a tilt of (*a*) normal to the loading axis and (*b*) 30 deg with respect to the loading axis.

fractograph (30 deg with respect to the loading axis) in Figure 6(b). In this case, the facet-forming primary-α is indicated on the side surface of the sample and can be seen to contain parallel slip marks. The surface crack initiation under the RS-free condition, therefore, can be considered as highly crystallographic in nature. In the same alloy at 23 °C and in the RS-free state, an increase in the incidence of subsurface-initiated failures was reported with a decrease in the stress level,[33] but at 860 MPa, a majority of failures were by a surface-initiation mechanism. It is a reasonable supposition that in Ti-6-2-4-6, in the absence of surface RS, the surface crack initiation in one or a few microstructural units will predominate, especially at an elevated temperature.

C. *Effect of SP on the Lifetime Distribution*

The SP treatment produces longer mean lifetimes, often by promoting subsurface crack initiation.[7,8] This is particularly the case in smooth-bar fatigue in the intermediate lifetime range, where in an otherwise RS-free condition, failure would occur by surface crack initiation.[6,15] At stress levels where significant mechanical relaxation of the RS is favored, failure by surface initiation is generally reported,[7,12,20,21] and the SP benefit to lifetime is nominally reduced. The emphasis in this study has been on the distribution in lifetime at an intermediate stress level, where a significant level of RS is retained under fatigue loading, and the dominant failure mechanism in the absence of RS is by surface crack initiation.

The lifetime distributions in microstructures A and B in the SP condition are compared to the RS-free state in Figure 7. The surface and subsurface failures have been depicted by open and closed symbols, respectively. Several key features of the fatigue variability behavior under SP are apparent from Figure 7. First, there is a clear benefit of SP in terms of the mean lifetime

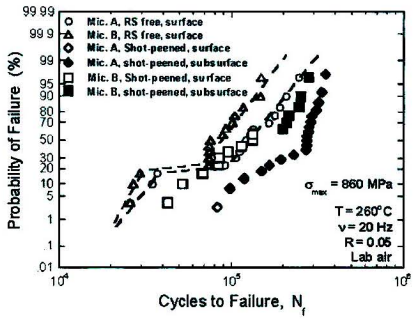

Fig. 7—Fatigue variability behavior in Ti-6-2-4-6 in the SP condition at 260 °C compared to the RS-free case.

behavior. Second, unlike the RS-free condition, the lifetime distributions under SP display segregation in terms of surface and subsurface-initiated mechanisms. Third, a strong role of microstructure in the probability of surface *vs* subsurface-initiated failure is evident, in that in the given number of experiments, crack initiation is driven to the subsurface in almost all experiments in microstructure A, but less than 50 pct of the tests in microstructure B.

Given the variability in the relaxed RS profile (Figure 4), an important consideration is whether the degree of relaxation correlates with lifetime. The crack initiation distance from the surface is plotted against lifetime in Figure 8(a), and the compressive RS upon relaxation (surface and maximum subsurface RS, which occurs at a depth just below the surface) is plotted in Figure 8(b) for selected samples in which the RS profiles were obtained. The points in Figure 8(b) represent only

the subsurface-initiated failures. The average depth of compressive RS upon relaxation is demarcated by the shaded area in Figure 8(a). Although the subsurface failures initiated beyond the compressive RS depth region, the center of crack initiation ranging from about 230 to 1748 μm from the surface, there is no clear relationship of the depth of initiation with lifetime. Furthermore, Figure 8(b) indicates that the retained nominal stress profile does not correlate with lifetime, and in these samples, subsurface initiation was favored across a wide range of values of the surface, or the maximum, compressive RS. This is not surprising, considering that, in the absence of RS, the surface crack initiation mechanism involves facet formation on the order of the equiaxed or lath α size, with the retained RS levels being more than sufficient in mitigating this mechanism.

An analysis of the effect of variability in the retained RS profile on the driving force for surface *vs* subsurface crack propagation will be presented in a forthcoming article. Given that surface crack initiation in the RS-free state involves crystallographic-facet formation on the size scale of a primary-α particle (about 10 μm), in spite of the variability in the RS relaxation, it is reasonable to expect the failure initiation to shift to the subsurface region, especially when a significant amount of compressive RS is retained. In this regard, the subsurface failures in Figure 7 can be considered as governed by the nominal RS profile. The surface failures, on the other hand, are suggested to arise due to more localized SP-material interaction events, as discussed in Section D. From a life-prediction perspective, this indicates that a probabilistic description of the fatigue response that integrates the nominally driven *vs* the locally controlled effects may provide a platform for including appropriate credit of a surface treatment in life prediction.

It is interesting that the probabilities of failure by surface crack initiation differ significantly between the two microstructures. It is not clear which microstructural characteristic controls this effect. As noted previously, the tensile behavior of the two microstructures was similar (Figure 2), and optically, they differed in terms of volume fraction of the primary α particles and aspect ratio of the secondary lath-α. However, the differences in terms of the crystallographic texture and the size and degree of microtexturing between the two may have had the strongest influence on the frequency of occurrence of local SP-affected regions that promote a condition for surface crack initiation. It is also useful to note the change in the slope of data points within the subsurface-initiation mechanism in microstructure A (Figure 7). This appeared to correspond to a switch in the nature of subsurface crack-initiation faceting and will be discussed in detail in another article.

D. *Nominal vs Life-Limiting Failure Mechanisms under SP*

Typical crack initiation characteristics in the RS-free case, presented in Figure 6, revealed facet formation in a surface α particle or α/β colony. As discussed previously, under SP, the lifetime distribution separated into subsurface and surface-initiated failures. These two modes of crack initiation in microstructure B are shown in Figures 9 and 10, respectively. Microstructure A also displayed the same crack initiation characteristics. The size (in terms of the diameter of a circle equivalent to the crack-initiation area) and the spatial angle of the crack-initiation feature with reference to the loading axis in representative samples of each microstructure are given in Figures 11(a) and (b), respectively. These figures illustrate the key contrasts between the nature of crack initiation under the RS-free and the SP condition, as discussed next.

As noted previously, the shift to subsurface initiation is expected under SP due to the small surface crack initiation size in the absence of surface RS and is considered to be the response to the nominal RS profile.

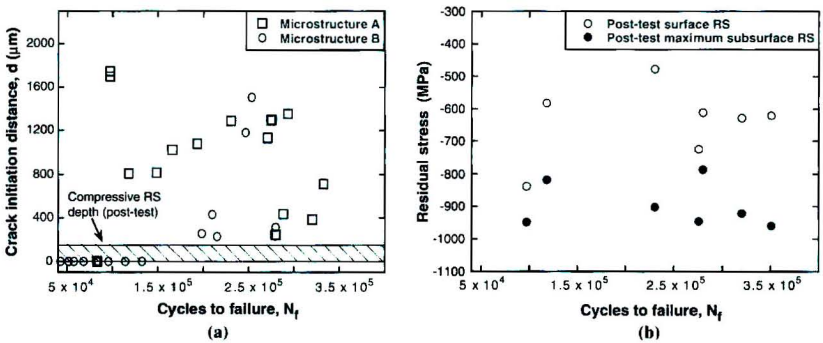

Fig. 8—Effect of the post-test RS level on the crack initiation distance from the surface and the lifetime. (*a*) Crack initiation distance *vs* lifetime and (*b*) surface and maximum subsurface RS level as a function of lifetime.

Figure 9(a) shows an overview of the subsurface initiation, where the center of crack initiation was approximately 315 μm from the surface, and indicates a significantly larger crack initiation area than in the RS-free case. In particular, in the RS-free condition, Figures 6 and 11 show that crack initiated within a single (or a few contiguous) microstructural unit (about 10 μm in equivalent diameter) by facet formation along a crystallographic plane that is at an angle of about 30 to 45 deg with respect to the loading axis (Figure 11(b)). The subsurface initiation under SP also occurred by crystallographic faceting (Figure 9(b)), such that the facet angles were approximately 30 to 50 deg with respect to the loading axis (Figure 11(b)), but in a collection of equiaxed and lath α spread over a much larger area with the equivalent diameter of about 100 to 200 μm (Figure 11(a)). It should be noted that the crack initiation size for subsurface initiation, plotted in Figure 11(a), was taken as the diameter of the circle equivalent to the polygon circumscribing the field of faceting at the crack origin. Multiple points at a given lifetime of a subsurface-initiated failure in Figure 11(b) represent the collection of facets forming a given crack initiation area.

The surface crack initiation mechanism under the SP is presented in Figure 10 and appears to have occurred by a large scale noncrystallographic fracture, in that the fracture was indiscriminant with respect to microstructural phases or crystallographic planes (Figure 10(a)). A switch in the fracture topology from nearly flat fracture morphology at the crack initiation site to the classical crack growth type morphology was observed, as approximately demarcated in Figure 10(a). Figure 10(b) shows the inverted version of the image in Figure 10(a), in which the average topographic differences between the crack initiation area and the crack growth region are more easily visualized. This is further illustrated with the help of the digital elevation map (DEM) of the crack initiation region (Figure 10(c)). The DEM was constructed by the quantitative tilt fractography technique employing the MeX 3D image analysis program (Alicona Imaging GmbH, Grambach, Austria). In Figure 10(c), the DEM is rotated counterclockwise by about 60 and 30 deg, respectively, with reference to the X-axis and Y-axis in the configuration shown in Figures 10(a) and (b) in order to provide a clearer visualization of the fracture features and the transition between the two types of morphologies. The ends of the crack initiation site have been indicated in Figures 10(a) through (c). The transition between the flat-fracture area and the metallic-crack-growth type morphology is clearly apparent in Figure 10(c). As shown, the shape of this area was invariably shallower in the depth direction than along the surface. The second key characteristic of the surface crack origin, evident in most cases, was that crack initiation was associated with a (or more) sharp roughness feature(s), as indicated in Figure 10(a) and shown in detail in Figure 10(d). In Figure 10(d), the sample is shown at a tilt of 45 deg with respect to the loading axis. The size of the noncrystallographic area was measured in representative samples and is plotted in Figure 11(a) in terms of the equivalent diameter, which was roughly between 60 and 200 μm. Further, Figure 11(b) depicts that the flat-fracture area was close to the normal to the loading axis.

Although near normal to the loading axis, given the radial crack growth patterns (Figure 10(a)), it appears that the flat region found in surface initiation sites may not have developed by instantaneous fracture across the entire area. While the surface layer has a nominal work hardening level, locally, the degree of hardening may fluctuate depending on the underlying microstructure.

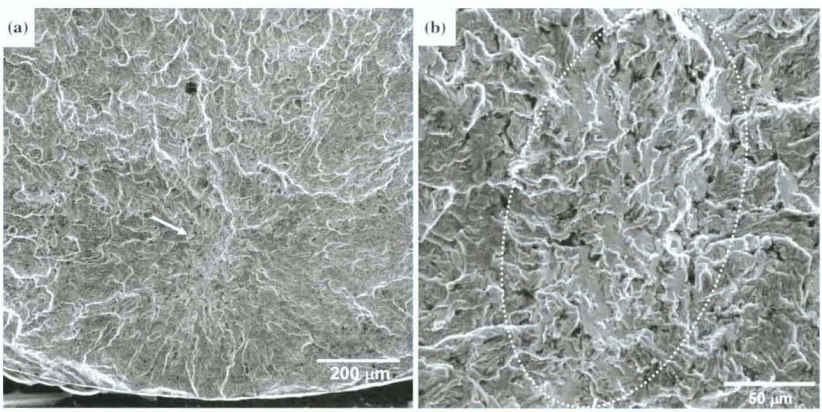

Fig. 9—Subsurface (center of crack initiation is about 315 μm from the surface) crack initiation under SP condition at 260 °C: (*a*) an overview of the crack origin and (*b*) crack initiation mechanism indicating a large field of α facet formation.

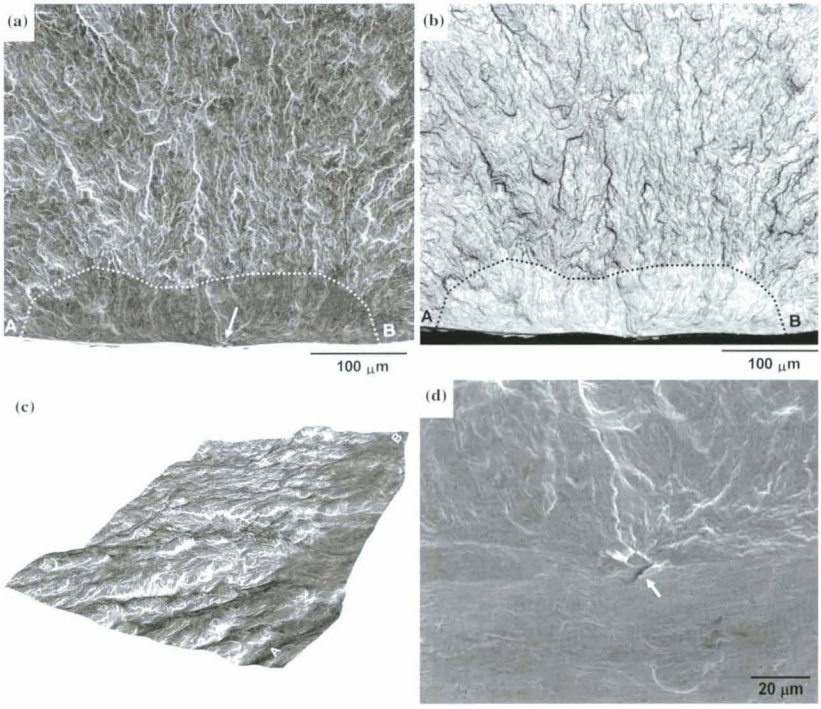

Fig. 10 Surface crack initiation mechanism under SP condition in microstructure B: (*a*) surface initiation site indicating a large noncrystallographic fracture area, (*b*) a version of the image in (a) where the colors have been inverted, (*c*) the digital elevation map of the crack initiation region revealing the transition between the flat fracture morphology and ductile crack growth, and (*d*) detailed view of the notchlike surface feature, where the sample is shown at a tilt of 45 deg with respect to the loading axis.

One possible mechanism of formation of the large noncrystallographic fracture area can be *via* rapid fatigue crack initiation and growth in a critically work-hardened location coincident with a notchlike roughness feature. The longer surface length than the depth of the flat region may also signify a rapid formation of this area, as opposed to formation by slow crack growth, in which the crack is generally found to grow significantly faster in the depth direction due to the RS gradient.[10] The surface crack initiation size under SP, plotted in Figure 11(a), pertains to this hypothesis and has been speculated to be effectively equivalent to the noncrystallographic, flat fracture area. However, as evident from Figure 10, due to the uncertainty in precisely determining the boundary between the noncrystallographic area and the ductile crack-growth morphology, the surface crack initiation sizes under SP in Figure 11(a) should be considered as approximate.

Given the preceding analysis of the competing nominal *vs* local effects of SP and associated crack initiation sizes and mechanisms, it can be emphasized that the nominal RS profile eliminates the crystallographic, microstructure-scale surface crack initiation mechanism in favor of a much larger scale crystallographic initiation from the subsurface. However, coexistent with this nominal-RS-driven behavior is another surface-initiated mechanism, attributed to randomly occurring localized surface events, by noncrystallographic crack initiation and significantly larger crack initiation size than in the RS-free case. Here, it is useful to note the peening configuration in terms of the shot size relative to the size and the geometry of the specimen. This is illustrated by Figure 3, where relative dimensions are to scale. Considering that spherical shots of diameter 0.5 mm were employed on a cylindrical specimen of about 4-mm diameter, the local SP-affected regions may be partly

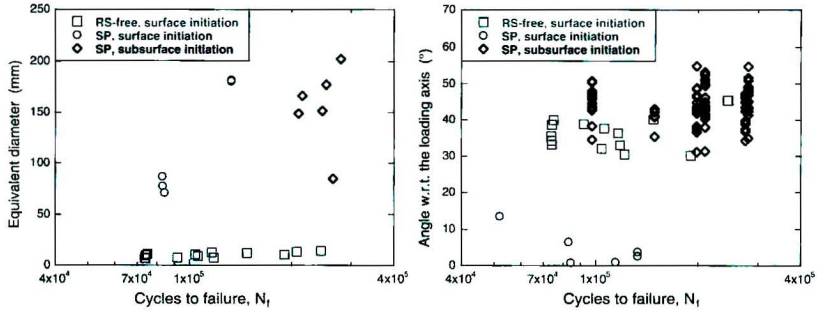

Fig. 11—Crack initiation characteristics under RS-free and SP conditions in Ti-6-2-4-6: (*a*) crack initiation size in terms of the equivalent diameter and (*b*) angle of fracture plane with respect to the loading axis.

contributed by the nature of contact between the shots and the specimen.

E. *Accounting for a Surface Treatment in Life Prediction*

This study shows that it may be useful in life prediction to consider a mean *vs* life-limiting description of fatigue variability in which the two behaviors respond differently to microstructure and extrinsic variables. Therefore, the effect of a surface treatment, such as SP, on a material has to be assessed both in terms of the influence on its mean lifetime and, more importantly, the impact on the lower tail of the lifetime distribution, which is controlled by factors very distinct from those governing the mean response and pursues a different crack initiation mechanism and size. For instance, in this approach, the effect of increased peening intensity on fatigue lifetime can be represented in terms of the separation of the effects of higher nominal RS level and the localized SP-process-induced factors. Thereby, while the former effect may increase the nominal lifetime, the latter might in fact increase the propensity for life-limiting, surface-initiated failures, due to increased possibility of localized work-hardened regions and surface notchlike features. Such lifetime trends with respect to the peening intensity have been reported by other researchers,[7] where a high SP intensity was shown to favor surface-initiated failures in rotating-bending fatigue, while an intermediate intensity produced the maximum benefit on lifetime by promoting subsurface failures in the majority of the samples (at lower stress levels).

Besides the separation into the two distributions, another key aspect in life prediction or the assessment of the effect of SP on lifetime, evident from this article, is that the surface crack initiation size is different for the RS-free and the SP cases. This needs to be accounted for in an accurate prediction of the lower tail of the lifetime distribution under the SP treatment.

Finally, it should be noted that the inherent, largely microstructurally promoted lower-tail-lifetime (or the life-limiting distribution) response being emphasized here is expected to arise in spite of an otherwise nominally perfect surface treatment. This is to draw a distinction with homogeneous extrinsic factors such as lack of perfect SP coverage and over-aggressive treatment, which have been reported by several researchers[34,35] to affect the average fatigue behavior. It is recognized, however, that these extrinsic effects may randomly occur in any surface and will complement the localized microstructural effects in driving the lower tail of lifetime.

V. SUMMARY

To summarize, this article demonstrates that the effect of a surface treatment such as SP on fatigue lifetime variability needs to be accounted for in terms of the nominal *vs* the local effects. In the present problem, the nominal RS levels induced by SP are found to drive the failure to the subsurface region, producing substantial lifetime benefits with reference to the RS-free case. However, the subsurface failure distribution was accompanied by the life-limiting distribution that was controlled by the local, SP-material interaction events, irrespective of the level of retained nominal RS level, and these failures approached the lifetimes under the RS-free condition. This nominal *vs* local effect was found to be strongly dependent on the microstructure, a further indication of the influence of local microstructure in producing the life-limiting crack initiation mechanism.

ACKNOWLEDGMENTS

This work was performed at the Air Force Research Laboratory, Materials and Manufacturing Directorate,

Wright-Patterson Air Force Base, OH. The financial support of the Air Force Office of Scientific Research (AFOSR) through AFOSR Task No. 92ML02COR, Dr. Victor Giurgiutiu and Dr. David Stargel, Program Managers, is gratefully acknowledged. We are also grateful for the partial financial support of the Defense Advanced Research Project Agency (DARPA) under DARPA orders M978, Q588, P699, and S271, Dr. Leo Christodoulou, Program Manager. We also acknowledge Dr. Dennis Buchanan of University of Dayton Research Institute for the very helpful discussions and for his assistance with RS measurements.

REFERENCES

1. *Shot Peening*, L. Wagner, ed., Wiley-VCH, New York, NY, 2002.
2. A. Drechsler, T. Dorr, and L. Wagner: *Mater. Sci. Eng.*, 1998, vol. A243, pp. 217–20.
3. J.D. Almer, J.B. Cohen, and B. Moran: *Mater. Sci. Eng.*, 2000, vol. A284, pp. 268–79.
4. E.R. De Los Rios, A. Walley, M.T. Milan, and G. Hammersley: *Int. J. Fatigue*, 1995, vol. 17, pp. 493–99.
5. R.K. Nalla, I. Altenberger, U. Noster, G.Y. Liu, B. Scholtes, and R.O. Ritchie: *Mater. Sci. Eng.*, 2003, vol. A355, pp. 216–30.
6. G.S. Was and R.M. Pelloux: *Metall. Trans. A*, 1979, vol. 10A, pp. 656–58.
7. M.A.S. Torres and H.J.C. Voorwald: *Int. J. Fatigue*, 2002, vol. 24, pp. 877–86.
8. J. Lindeman, C. Buque, and F. Appel: *Acta Mater.*, 2006, vol. 54, pp. 1155–64.
9. R. John, J.M. Larsen, D.J. Buchanan, and N.E. Ashbaugh: *Incorporating Residual Stresses in Life Prediction of Turbine Disks*, NATO RTO (AVT) Symp. on Monitoring and Management of Gas Turbine Fleets for Extended Life and Reduced Costs, Manchester, UK, Oct. 8–11, 2001.
10. M. Beghini, L. Bertini, and E. Vitale: *Fatigue Fract. Eng. Mater. Struct.*, 1994, vol. 17, pp. 1433–44.
11. C.H. Wang, S.A. Barter, and Q. Liu: *J. Eng. Mater. Technol.*, 2003, vol. 125, pp. 183–90.
12. G.A. Webster and A.N. Ezeilo: *Int. J. Fatigue*, 2001, vol. 23, pp. S375–S383.
13. E. Hornbogen, M. Thumann, and C. Verpoort: *Proc. 1st Int. Conf. on Shot Peening*, ICSP 1, Pergamon Press, Oxford, United Kingdom, 1987, pp. 381–87.
14. A. Turnbull, E.R. De Los Rios, R.B. Tait, C. Laurant, and J.S. Boabaid: *Fatigue Fract. Eng. Mater. Struct.*, 1998, vol. 21, pp. 1513–24.
15. R.C. McClung: *Fatigue Fract. Eng. Mater. Struct.*, 2007, vol. 30, pp. 173–205.
16. Y. Mutoh, G.H. Fair, B. Noble, and R.B. Waterhouse: *Fatigue Fract. Eng. Mater. Struct.*, 1987, vol. 10, pp. 261–72.
17. E.R. De Los Rios, M. Trull, and A. Levers: *Fatigue Fract. Eng. Mater. Struct.*, 2000, vol. 23, pp. 709–16.
18. C.A. Rodopoulous, S.A. Curtis, E.R. De Los Rios, and J. Solisromero: *Int. J. Fatigue*, 2004, vol. 26, pp. 849–56.
19. Z.L. Lu, S.X. Li, Y.Y. Lui, Q.Y. Zhang, J.F. Lei, and Z.X. Mu: *Mater. Sci. Eng.*, 2004, vol. A383, pp. 283–88.
20. M.C. Berger and J.K. Gregory: *Mater. Sci. Eng.*, 1999, vol. A263, pp. 200–04.
21. W.Z. Zhuang and G.R. Halford: *Int. J. Fatigue*, 2001, vol. 23, pp. S31–S37.
22. B.L. Boyce, X. Chen, J.O. Peters, J.W. Hutchinson, and R.O. Ritchie: *Mater. Sci. Eng.*, 2003, vol. A349, pp. 48–58.
23. D.J. Buchanan and R. John: *Scripta Mater.*, 2008, vol. 59, pp. 286–89.
24. R. John, D.J. Buchanan, S.K. Jha, and J.M. Larsen: *Scripta Mater.*, 2009, vol. 61, pp. 343–46.
25. S. Curtis, E.R. de Los Rios, C.A. Rodopoulos, and A. Levers: *Int. J. Fatigue*, 2003, vol. 25, pp. 59–66.
26. G.R. Leverant, B.S. Langer, A. Yuen, and S.W. Hopkins: *Metall. Trans. A*, 1979, vol. 10A, pp. 251–57.
27. S.K. Jha, M.J. Caton, and J.M. Larsen: *Mater. Sci. Eng. A*, 2007, vols. A468–470, pp. 23–32.
28. S.K. Jha, M.J. Caton, and J.M. Larsen: in *Superalloys-2008*, R.C. Reed, K.A. Green, P. Caron, T.P. Gabb, M.G. Fahrmann, E.S. Huron, and S.A. Woodard, eds., TMS, Warrendale, PA, 2008, pp. 565–72.
29. S.K. Jha and J.M. Larsen: *VHCF-4*, Proc. 4th Int. Conf. on Very High Cycle Fatigue, Ann Arbor, MI, 2007, J.W. Jones, J.E. Allison, J.M. Larsen, and R.O. Ritchie, eds., TMS Publications, 2007, pp. 385–96.
30. S.K. Jha, J.M. Larsen, and A.H. Rosenberger: *Eng. Fract. Mech.*, 2009, vol. 76, pp. 681–94.
31. C.J. Szczepanski, S.K. Jha, J.M. Larsen, and J.W. Jones: *Metall. Mater. Trans. A*, 2008, vol. 39A, pp. 2841–51.
32. P.S. Prevey: in *Developments in Materials Characterization Technologies*, C. Vander Voort and J. Friel, eds., ASM INTERNATIONAL, Materials Park, OH, 1996, pp. 103–10.
33. S.K. Jha, J.M. Larsen, A.H. Rosenberger, and G.A. Hartman: *Scripta Mater.*, 2003, vol. 48, pp. 1637–42.
34. L. Wagner and G. Lutjering: *Proc. ICSP-2*, Chicago, IL, May 14–17, 1984, American Shot Peening Society, NJ, pp. 194–200.
35. J.T. Cammett, P.S. Prevey, and N. Jayaraman: *Proc. ICSP-9*, Paris, France, September 6–9, 2005, American Shot Peening Society, NJ.